Proceedings World Geothermal Congress 2020+1
Reykjavik, Iceland, April - October 2021

Connectivity and Fault-Controlled at Different Scales: An Example from Fractured Geothermal Systems in the Southern Andes

Josefa Sepúlveda[a,b,*], G. Arancibia[a,b], T. Roquer [a,b], E. Molina[a,b], E.A. Veloso[a,b], D. Morata[b,c], J.V. Rowland.

[a]Departamento de Ingeniería Estructural y Geotécnica, Pontificia Universidad Católica de Chile, Av. Vicuña Mackenna 4860, Macul, Santiago, Chile.

[b]Centro de Excelencia en Geotermia de los Andes (CEGA, FONDAP-CONICYT), Universidad de Chile, Plaza Ercilla 803, Santiago, Chile.

[c]Departamento de Geología, Universidad de Chile, Plaza Ercilla 803, Santiago, Chile.

*Corresponding author: jbsepulveda@uc.cl

Keywords: Liquiñe-Ofqui Fault System, Andean Transverse Faults, Connectivity, Fault-controlled fluid circulation.

ABSTRACT

Fault zones play an essential role in the spatial distribution of the geothermal resources in crystalline rocks (non-porous media). They can control the location, emplacement and evolution of geothermal systems by acting as barriers and conduits to geothermal fluid circulation through the crust, generating a fractured natural system. So, it is critical to study the nature of the fault control permeability in low porous crystalline rocks at different scales because different processes associated with the failure of rocks promote a complex time-dependent and enhancing/reducing the fluid flow pathways and are occurring in all scales. Furthermore, the fracture is connected between them forming a network, and if it is well-connected, the network will favor the fluid circulation through open fractures. Southern Volcanic Zone (Chile) was selected as a case of study to evaluate the role of the structural permeability in low porous crystalline rocks corresponding to the North Patagonian Batholith. Previous studies propose a relatively well-constrained first-order role of two active fault systems in fluid flow at crustal scales: 1) the arc-parallel Liquiñe-Ofqui Fault System (LOFS) with an NS to NNE trending, and 2) the arc-oblique Andean Transverse Faults (ATF) with an NW trending. Now, it is proposed to examine the Liquiñe area (~39°S) as the site of interaction between these active fault systems and the spatial localization of the several hot springs in order to evaluate this natural fractured geothermal system. For that, this study is focused on one representative outcrop of the ATF, analyzing the fracture features in thin sections and the outcrop (millimetric to centimetric scale), and following the methodology proposed by Sanderson and Nixon (2015). The main results indicate that at centimeter-scale, the fractures are well connected with a connectivity per branch of 2.0 and Y-nodes is the primary node type, meanwhile, at millimeter-scale, the connectivity was 1.85, and the predominate node is also the Y-node. So, as much the pattern network and connectivity are similar at both scales, but the density and intensity of fractures are overestimated at smaller scales. Moreover, the fracture network in the selected outcrop is well-connected, allowing the fluid circulation. Finally, for future works, we will considerer more areas at different scales to analyze the connectivity.

1. INTRODUCTION

The geothermal energy is a sustainable and renewable energy source, and it is concentrated in zones where the geothermal gradient is anomalously higher (> 30 ºC) such as subduction zones or volcanic arcs (Moeck, 2014; Sánchez et al. 2015). Every geothermal system needs a permeable volume of rock that stores the hot fluids and allows the circulation of this fluid through rocks (e.g., Moeck, 2014). However, when the host rock has low porosity, the permeability will be conditioned by the connection of fractures. In particular, fault zones in the crust are interesting because, in these zones, the fracture density and the connection between them are increased, favoring the permeability in crystalline rocks (Sibson, 1996; Cox, 1999).

A fault zone is composed of a central volume of rock named fault core where most of the displacement is accommodate, and it could contain a simple core or multiples cores. Around this, there is a damage zone which consists in a network of subsidiary faults and fractures (not sealed or sealed with secondary minerals) at a range of different lengths (Caine et al., 1996; Chester and Logan, 1986; Faulkner et al., 2003; Gudmundsson et al., 2001). Different authors have suggested that the mechanical and hydraulic properties are spatially and temporally associated to the fault zones (Faulkner and Rutter, 2001) and for example, the density of fractures and faults, and permeability decrease exponentially with distance from the fault core increases (Faulkner et al., 2010).

In zones where the fracture density is relatively high, the fractures are connected, forming a network. It is essential in low porosity rocks, where the connections between fractures determine the permeability and fluid circulations. The pattern of the fracture network has significant consequences in the mechanical properties of the rock and fluid transport through rocks, mainly because the connectivity determines if the network is well or poorly connected. Different authors have reported that the pattern network is repeated at different scales (e.g., Bonnet et al., 2001; Bour et al., 2002; Davy et al., 2006). It is well known that the fracture length distribution is similar at different scale and defined by a power-law distribution in most cases. However, other second features such as connectivity are contributed to the permeability of the system (Long and Billaux, 1987), and also it is similar at different scales (Mauldon et al., 2001; Davy et al., 2006), what is relevant because both micro-connectivity and macro-connectivity contributes to the permeability. However, those features are less studied than the fracture length distribution.

A way to study the connectivity of a fracture network is through the topology, which is the relationship between different geometric attributes of fractures (Manzocchi, 2002; Sanderson and Nixon, 2015). The interaction between the features is the key to understand why some fractures networks are better to conduct the fluids through fractures, and others are better for storage. For example, two

fracture networks could have the same quantity of fractures with the same orientation and the same length, but the spatial distribution and the connections can vary between them and therefore the permeability would be different for these two fracture networks (Figure 1). So, the topology is a way to understand how the fracture network and its features affect fluid circulation (Sanderson & Nixon, 2015).

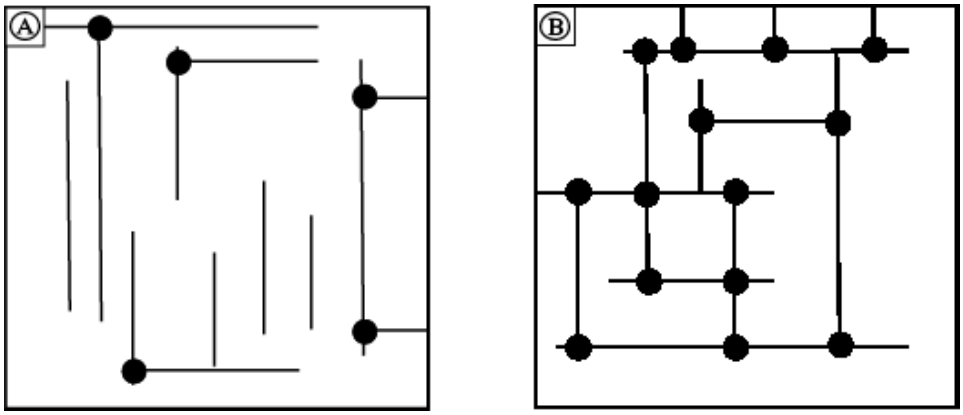


Figure 1: Example of the connectivity in fractures networks. In this example, A and B have the same number of fractures but different spatial distribution, allowing that B has larger connectivity than A.

Moreover, the understanding of the fracture network at different scales is essential to characterize a system, especially in a geothermal project where the permeability is given by the connectivity between fractures. It also allows us to understand how fluids are stored and circulate through the fracture system.

An excellent case to study the effects of the fracture connectivity in the fluid circulation is the Andean Southern Volcanic Zone (SVZ) where the geothermal potential is high, and it was estimated varying between 600 and 1400 MWe (Barbier, 2002; Aravena et al., 2016; Lahsen et al., 2010). Moreover, the basement of the volcanic arc is composed of low porous rocks, principally granitic rocks, and fractures networks control the permeability.

The aim of this study is how is the connectivity of the fracture network of Liquiñe Geothermal System at two different scales. For this, a centimeter and millimeter areas were chosen in a representative outcrop from one of the main fault groups in the Liquiñe area (39 ºS) and the topology methodology proposed by Sanderson and Nixon (2015) was applied for both areas.

2. CASE OF STUDY

The SVZ is an active magmatic zone where the oblique convergence controls the tectonic of the zone, and it produces the partition of the deformation into a margin-parallel and margin-orthogonal components, which is accommodated within the arc and forearc, respectively (Figure 2-a) (e.g., Arancibia et al., 1999; Cembrano et al., 1996; Stanton-Yonge et al. 2016). The basement of the volcanic arc of the SVZ corresponds to the North Patagonian Batholith (NPB), a group of Jurassic to Miocene tonalitic to granodioritic bodies (Munizaga et al., 1988; Pankhurst et al., 1992; Pankhurst et al., 1999). Two groups of faults cut the NBP: 1) the Liquiñe-Ofqui Fault System (LOFS) and, 2) the Andean Transverse Faults (ATF). The LOFS is a fault system with 1200 km of length. It is formed by a master fault, which is NS- NNE-striking dextral to dextral-reverse, and subsidiaries faults that are NE to ENE-striking dextral and dextral normal (Cembrano et al., 1996; Arancibia et al., 1999; Cembrano and Lara, 2009). The ATF is NW to WNW-striking sinistral, and sinistral-reverse faults distributed through the Andes (Melnick et al., 2006; Rosenau et al., 2006, Cembrano and Lara, 2009; Pérez et al., 2016).

In Liquiñe (39 ºS), an area of the SVZ (Figure 2-a and b), the Paleozoic metamorphic rocks have been intruded by Jurassic, Cretaceous, and Miocene intrusive bodies belong to the NPB. Over these intrusive bodies, different Quaternary volcanic rocks from SVZ are deposited (Lara and Moreno, 2004). Furthermore, the thermal springs are spatially related to both the intrusive rocks of the NPB and these two main groups of faults. The depth of this geothermal reservoir has been estimated between 1 to 3 km (Sánchez et al., 2013) and the temperature of the reservoir, in this area, has been estimated varying between 80 ºC to 150 ºC and the fluid residence time is about 500 years (Sánchez et al., 2013; Held et al., 2018).

In this work, we study the connectivity between fractures in a Miocene granodiorite. It is a medium-grain size varying between 0.3 mm to 4 mm, and the granodiorite is composed by quartz (25%), plagioclase (35%), k-feldspar (20%), biotite replaced by chlorite (13%), altered amphibole (5%) and opaque minerals (2%). The rock is also cut by veins filled with epidote and subordinate chlorite with an aperture of 0.05 to 0.2 mm. Intercrystalline fractures appear around the borders of plagioclase, quartz and k-feldspars crystals, and also, a minor proportion of intracrystalline fractures were observed in plagioclases and k-feldspars crystals.

Additionally, one representative outcrop was selected (blue light star in Fig. 2-b). Faults planes, fractures and dikes cut the rock, and it is also cut by millimetric veins of epidote and subordinated chlorite. Additionally, different centimeter faults zones are an exhibit; some cataclastic bands are in the core of the fault zones. This outcrop was chosen because it is located in a fault zone of the ATF and the fracture density is high in the whole outcrop and it is aligned with a thermal lineaments N70W, which could represent an ATF lineament.

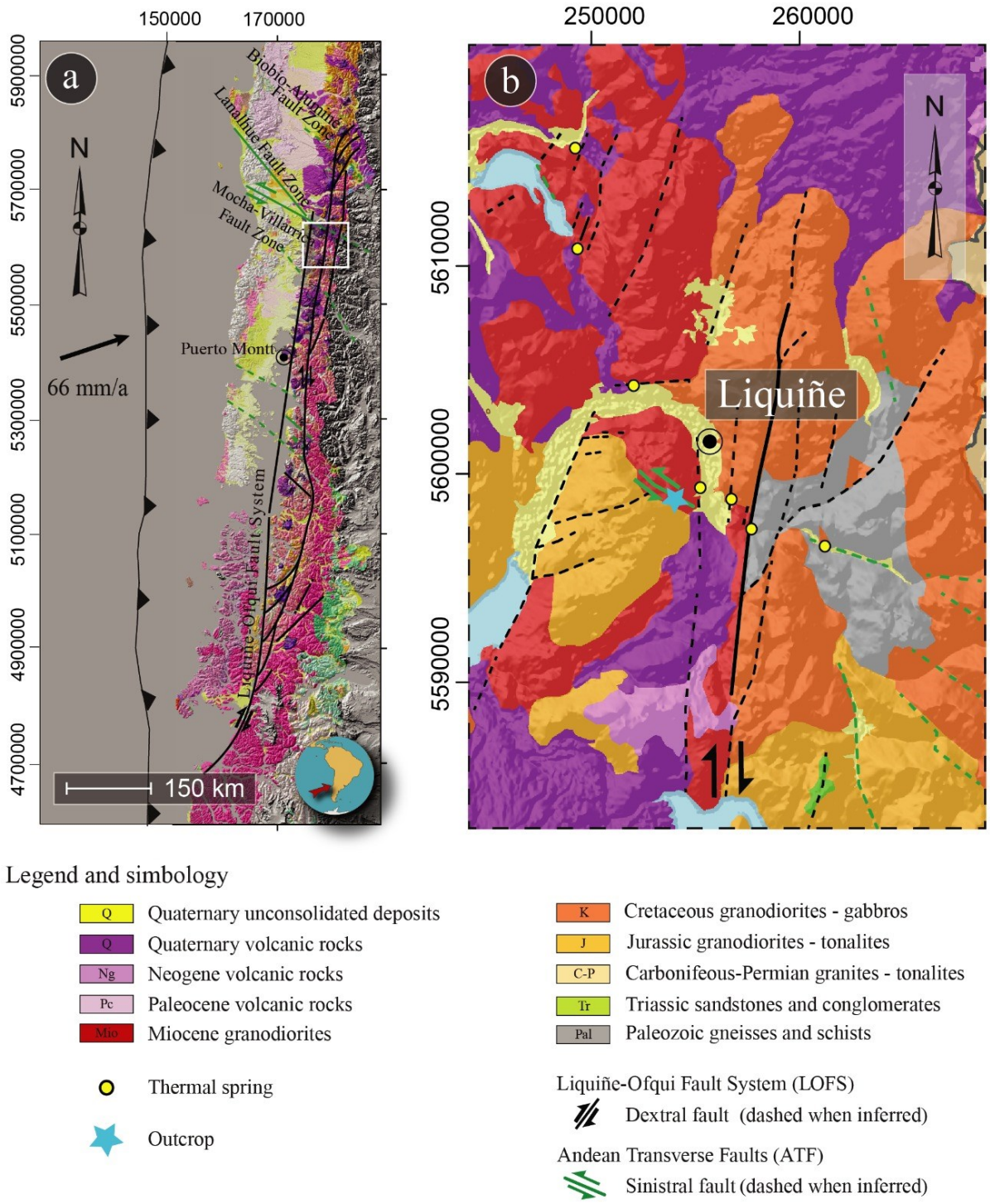


Figure 2: a) Regional geological map of the Southern Volcanic Zone, where the oblique subduction is 66 mm/yr and the volcanic arc basement is indicated in pink. b) The geological map of Liquiñe, the light blue star, indicates the selected outcrop "Cachim". The maps were modified from Lara and Moreno (2004), Rossenau et al. (2006), Sánchez et al. (2013) and Pérez-Flores et al. (2016).

3. METHODOLOGY

In this work, two scales were used to measure the topology at the outcrop scale and thin section scale in a representative outcrop called "Cachim" (light blue star, Fig. 2-b). This site was selected because it is a fault zone associated with the ATF and the density of fractures is enough to the methodology followed.

The topology and connectivity were estimated using a circular area because different authors have suggested that this shape is better than the square area because it reduces the bias effect on the fracture's measurements (Mauldon et al., 2001; Watkins et al., 2015). Moreover, the size of the dimeter's circumference at the outcrop scale was determined in order to represent a line that has all

orientations equally represented (in 2-dimensions) and, hence, the potential to provide less biased samples than straight lines (Sanderson and Nixon, 2015).

Then, the length fracture inside of the circumference was characterized and the intensity, density and mean length for each area (outcrop and thin section) were estimated. The intensity of fractures was defined like the total sum of the individual length fractures divided by the area (mm/mm^2), the density was the number of fractures divided by the area (mm^{-2}) and the mean length was the mean length of the all fractures inside of the circumference (e.g., Rohrbaugh et al., 2001; Gomila et al., 2016).

Once the areas were selected, three kinds of nodes were counted and those correspond to 1) I-node, which is a starting or ending node; 2) X-node, which correspond to an interception between two fractures and they form a cross ; 3) Y-node is the interception between two fractures, but one of them start or end in this interception forming a "Y" (see Figure 3) (Manzocchi, 2002; Nyberg et al., 2018; Sanderson and Nixon, 2015). Furthermore, the fractures were represented by lines and the interception of these fractures form branches, which is a piece of line bounded by two nodes (see figure 3). Different authors have suggested that topology and connectivity are better to understand considering branch than fractures because the size of the fractures most of the cases exceed the analyzed area. Also, the connectivity is defined by the connection of fractures, but not by the quantity of line.

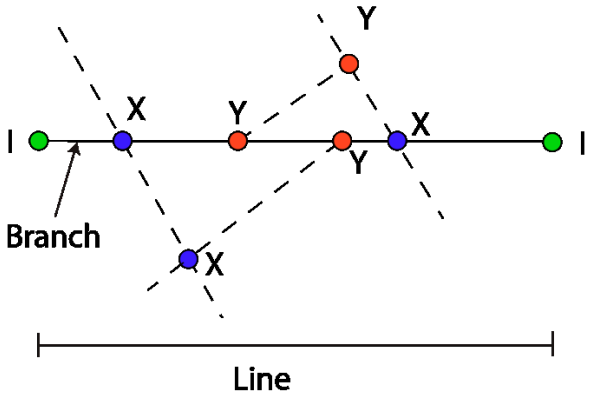


Figure 3. Node classification. The blue circles indicate X nodes, red circles indicate the Y-node and green circles indicate I-node. Modified from Sanderson and Nixon (2015).

Therefore, the topology is defined by the amount and the type of nodes, so different parameters were estimated from the sum of each node. First, it can be calculated the number of nodes (N_n) by the equation [1],

$$N_n = N_I + N_Y + N_X \qquad [1]$$

where N_I, N_Y and N_X are the number of I, Y, and X nodes, respectively.

The number of lines (N_L) was calculated using equation [2]. It only considered Y-nodes and I-nodes because these nodes define the beginning or end of one line. The number of branches (N_B) was calculated from equation [3], considering that I-node only produced one branch, Y-node divided the lines into three branches and X-node divided the lines into four branches. On the other hand, the number of connections (N_C) was calculated from the sum between Y-nodes and X-nodes (equation 4) (Nyberg et al., 2018), because only these types of nodes contributed to the connection.

$$N_L = \frac{N_Y + N_I}{2} \qquad [2]$$

$$N_B = \frac{N_I + 3N_Y + 4N_X}{2} \qquad [3]$$

$$N_C = N_Y + N_X \qquad [4]$$

Additionally, the connection per line (C_L) was calculated using the equation [5], and it only considers nodes y and x because they are connected by fractures. The connection per branch (C_B) was calculated from equation [6], and it considered a similar relation than equation [3]:

$$C_L = \frac{2(N_X + N_Y)}{N_L} \qquad [5]$$

$$C_B = \frac{3N_Y + 4N_X}{N_R} \qquad [6]$$

The studied outcrop is shown in Figure 4-a. In this case, a circumference of 28 cm in diameter was selected to delimit an area, which will be referred to as the “outcrop area” (Fig. 4-b). Then, in the thin section, a circumference of 1.2 mm in diameter was selected and it will be referred to as “thin section area” (Fig. 4-c). Respect to the outcrop area, open fractures and faults were only considered and they were projected in a plane where the topology and connectivity were calculated. Meanwhile, for the case of the thin section area, only open fractures were considered to the study of topology and connectivity, non-considering veins filled by epidote. For that, the number of fractures inside of these two areas was described only considering the length, and this parameter was measured using the software FRAPAQ (Healy et al., 2017).

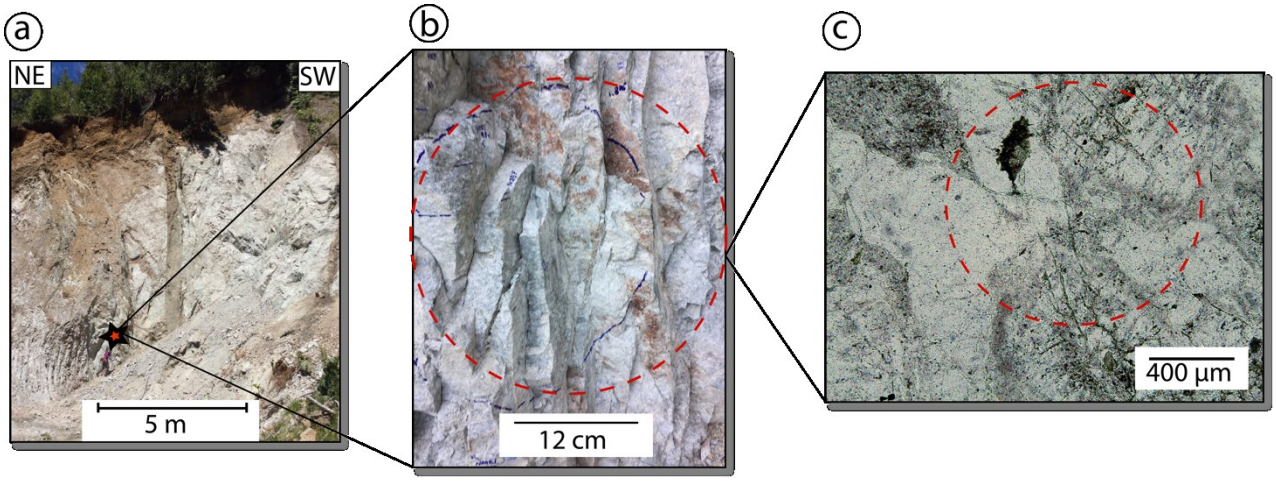


Figure 4. The selected outcrop area in the Cachim quarry (a), where a circumference methodology (red circle) to measure the connectivity was used at outcrop scale (b) and thin section scale (c).

4. RESULTS

In the outcrop area, the fracture's length inside of the circumference varies between 7.5 cm to 46 cm and the mean length is 15.7 cm. Additionally, the aperture varies from 0.1 to 0.6 cm, but it is variable along with the elements. Particularly, the aperture of fault planes was not possible to measure because it is an exposed plane and the other face was missed (Fig. 5a). In figure 5, the red circle indicates the area in a study where the nodes were counted in each case.

A thin section scale, the fractures are principally intercrystalline and they are between plagioclase, quartz and k-feldspars crystals, as is explained above. The length of these fractures varies between 0.028 mm to 0.56 mm. There is not a preferential direction because fractures are around minerals, and the variation of the aperture is from 0.006 mm to 0.017 mm. Furthermore, some clusters of fractures are observed in the thin section related to plagioclase and k-feldspars crystals (Fig. 5b).

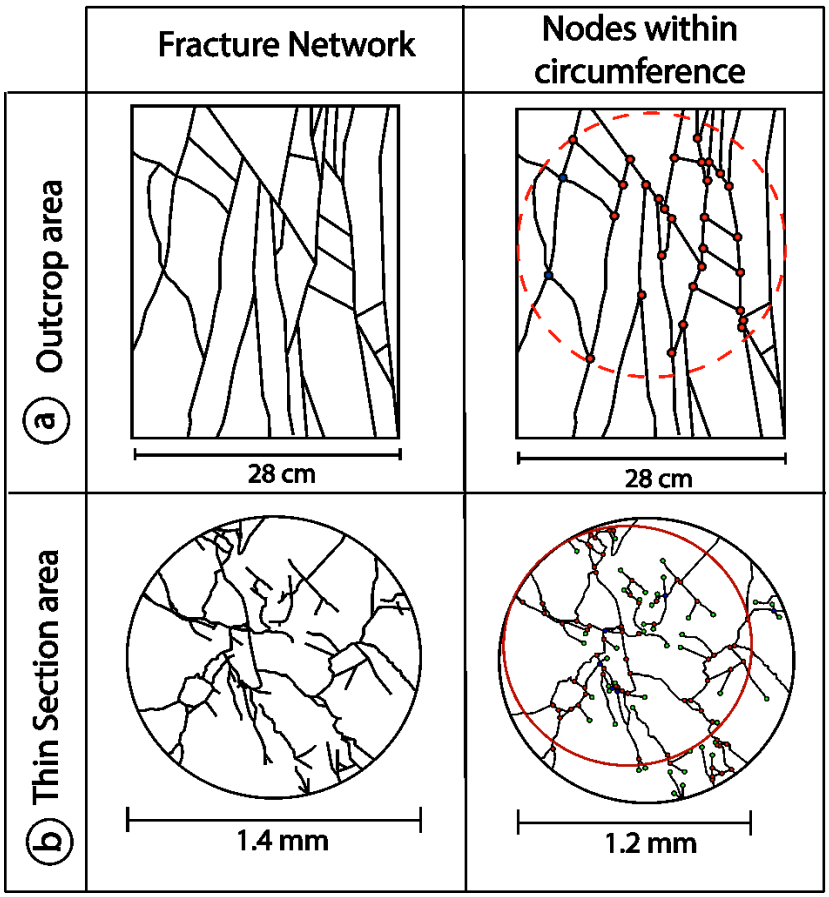


Figure 5. Fracture networks at both scales of work, outcrop and thin sections areas, first and second row, respectively. The first column corresponds to the fracture networks in each scale, and in the second column is shown the nodes I, X and Y counted for each case.

The results of the outcrop area only present two X-node, 29 Y-nodes and zero I-node (Fig. 6a). The total of nodes is 31, the total number of branches is 47.5, the total of lines is 14.5. The connectivity per line is 4.27, the connectivity per branch is 2.0 (Figure 6b) and the ratio between NB and NL is 3.3. In the thin section area, 4 X-nodes, 29 Y-nodes and 8 I-nodes are considered (Fig. 6c). Moreover, the total number of nodes is 39, the total number of branches is 52.5 and the total of lines is 17.5. The connectivity per line is 3.5, the connectivity per branch is 1.85 (Figure 6d), and the ratio between NB and NL is 3.

The fracture density in the outcrop area is 4.0×10-4 mm^{-2} and the intensity of fracture is 0.045 mm/mm^2. On the other hand, in the case of the thin section, the fracture density is 15.8 mm^{-2} and the intensity of fracture is 9.6 mm/mm^2. When those parameters were calculated only considering the pixel as length unit, the fracture density for the outcrop area was 5.4×10^{-4} px^{-2}, and the fracture intensity is 0.05 px/px^2, respect to the thin section area, that the fracture density is 8.6×10-4 px^{-2} and the fracture intensity is 0.033 px/px^2.

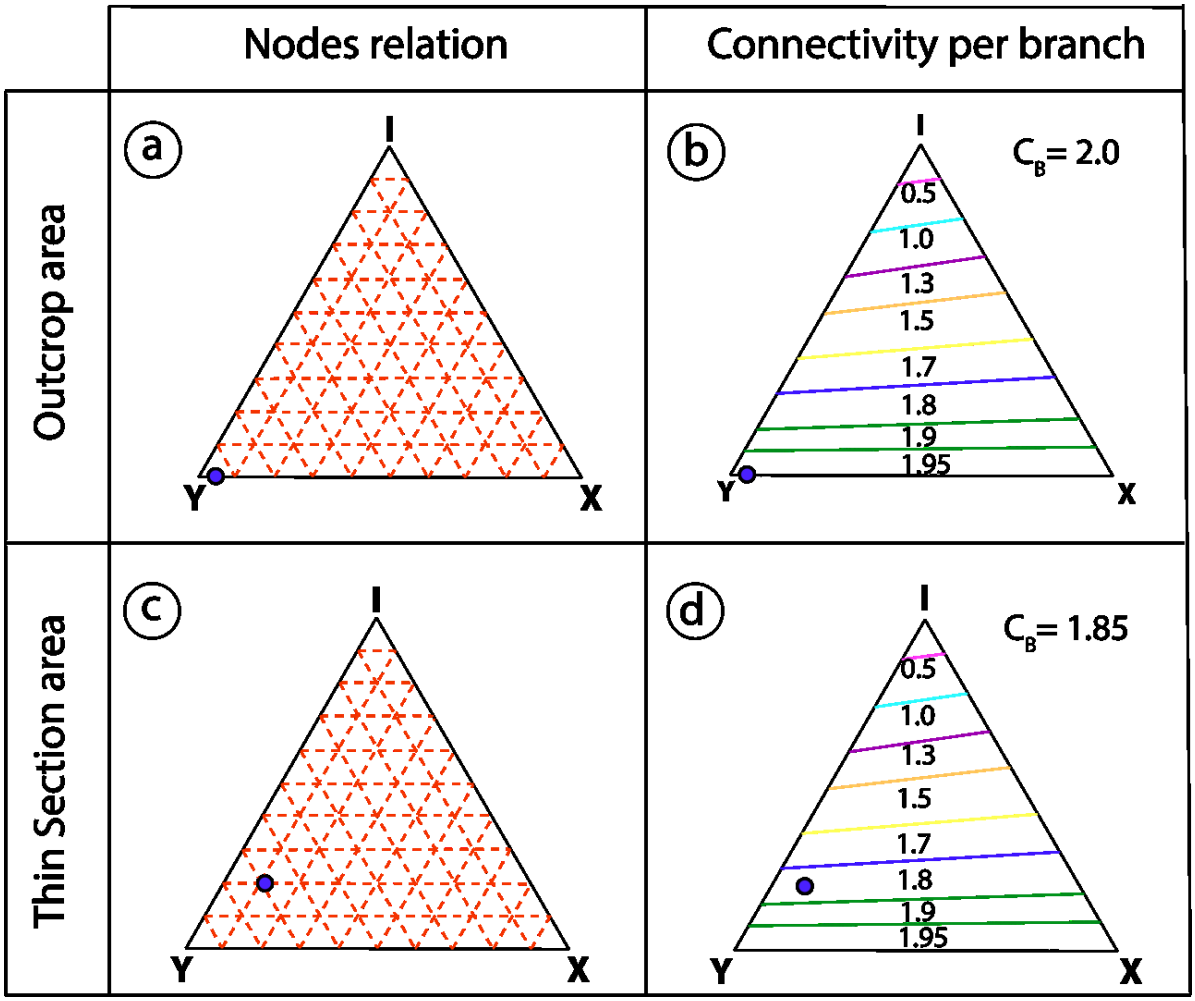


Figure 6. The nodes relationship in the outcrop area (a) and in thin section area (c), and their respective value of connectivity per branch (b and d).

5. DISCUSSIONS

The main node type is Y-node in both outcrop and thin section areas, and both networks also have low I-nodes. This proportion is according to the idea that more Y-nodes imply less isolated nodes, and therefore, it has a significant contribution to fracture connections because Y-nodes increase the connectivity (Manzocchi, 2002). Moreover, and according to with Sanderson and Nixon (2015), they suggested when the NB/NL ratio is similar to ~3, such as in these cases, it is expected a better connectivity improving in Y-networks because this type of node divides the lines into three branches (Sanderson and Nixon, 2015). Additionally, the high connectivity (C_B and C_L) in both studied areas indicate a well-connected fracture network. Additionally, after considering only open fractures, large connectivity implies a good network for fluid circulation (Sanderson and Nixon, 2015).

The connectivity in each network is shown in Fig. 7, where nodes I-I means a poor-connected network where the predominant nodes are the isolated nodes (I). The I-C is a partly-connected network, where the three kinds of nodes are found, and the C-C connection implies a well-connected network because it considers Y-X nodes. In this case, both the outcrop area and the thin section area represent a well-connected network, as previously commented.

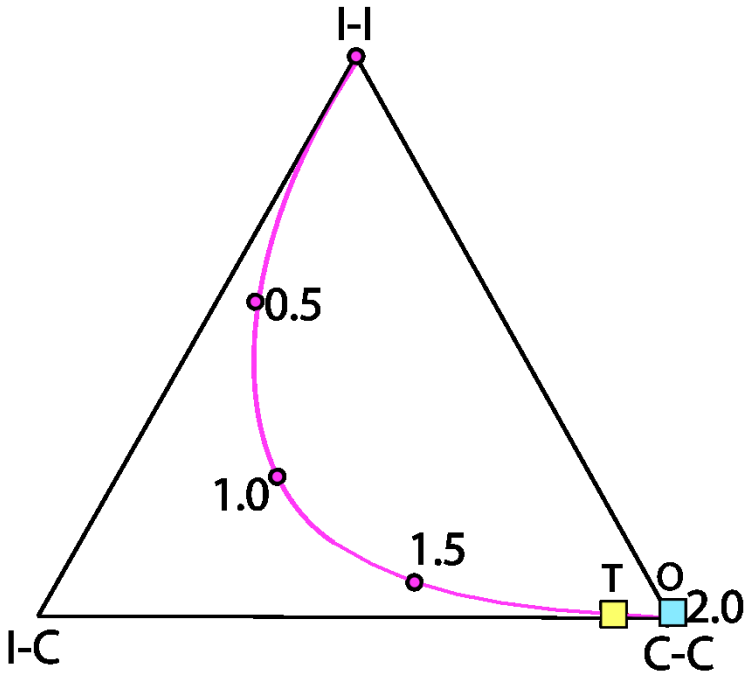


Figure 7. Connection of the network according to the type of nodes. In this figure, the light blue square (O) represents the connectivity in the outcrop scale and yellow square (T) represents the connectivity at a thin-section scale.

In the same line, the pattern network is replied at different scales analyzed in this work. It is reflected in the fact that similar proportions of Y, X, and I nodes are in the selected areas, and also, the connectivity per branch is similar between them (C_B ~2). So, the topology, network pattern, and connectivity are replicable in these two used scales, implying that these parameters could be extrapolated for larger scales to study the permeability of the system and to understand how the fluid circulation is occurring.

The density and intensity of fractures decrease at larger scales, which is according to Rohrbaugh et al., 2001 because, in smaller areas, the density is overestimated. However, when the density and intensity are estimated in the function of pixels (as length unit), the values of intensity are similar, which indicates that the portion of fractures in comparison with the area are proportional in both scales (outcrop and thin section areas). Nevertheless, it is essential to analyze more areas at other scales to have a better estimation. So, in future work, we must considerer new outcrops (from centimetric to metric scale) and the respectively thin section of each outcrop and, additionally considering different diameters to measure the topology and connectivity.

This work was focused in exposed areas, so to understand the behavior of the topology and connectivity in-depth, and how fluid is transported through the fracture networks, it is important to considerer that those parameters are influenced by other intrinsic factors of fracture such as tortuosity, aperture and filling, as well as external factors like depth, differential pressure, temperature and fluids viscosity (i.e., Sibson et al., 1996; Cox, 1999; Fossen, 2010). These factors, both intrinsic and external, were not considered in this study. Furthermore, the fluid circulation is conditioned by the tectonic effects because it conditions the structural geology of the area, as for an example, the LOFS and ATF. The orientation and the interaction of those faults will condition the fluid circulation in this geothermal system. In that sense, different authors have suggested that the orientation of the LOFS respect to the direction of the regional stress is favoring the fluid circulation, while the ATF respect to orientation of the regional stress is favoring the storage of fluids (Tardani et al., 2016, Pérez Flores et al., 2016).

6. CONCLUSION

In this work, a representative outcrop of the ATF was selected to estimate the topology and connectivity at millimetric and centimetric scales. The connectivity is similar at both scales and indicates a well-connected fracture network, which could favor the fluid circulation through this network. Furthermore, at both scales, the Y-node is the primary type of nodes indicating that the patter of fractures networks is similar at both scales. Hence, those results indicate that the properties are replicable at different work scales. Finally, it is the first approximation of connectivity in one outcrop of the Liquiñe area, but more areas at different scales must be considered in future works, and also must be necessary include other host rocks presented in this area to have a more realistic estimation of the connectivity of the Liquiñe Geothermal Systems.

ACKNOWLEDGMENTS

This research was supported by FONDECYT Regular project Nº1180167 and FONDAP-CONICYT project N°15090013 "*Centro de Excelencia en Geotermia de los Andes*" (CEGA).

REFERENCES

Arancibia, G., Cembrano, J., Lavenu, A. Transpresión dextral y partición de la deformación en la Zona de Falla Liquiñe-Ofqui, Aisén, Chile (44–45ºS). *Revista Geológica de Chile*, **26** (1999), 03-22.

Aravena, D., Muñoz, M., Morata, D., Lahsen, A., Parada, M. Á., and Dobson, P.: Assessment of high enthalpy geothermal resources and promising areas of Chile, *Geothermics*, **59** (2016)., 1–13.

Barbier, E., and Barbier, E.: Geothermal energy technology and current status: an overview, *Renewable and Sustainable Energy Reviews*, **6** (2002)., 3–65.

Bonnet, E., Bour, O., Odling, N. E., Davy, P., Main, I., Cowie, P., & Berkowitz, B.: Scaling of fracture systems in geological media. *Reviews of Geophysics*, **39** (2001), 347–383.

Bour, O., Davy, P., Darcel, C., Ödling, N.: A statistical scaling model for fracture network geometry, with validation on multiscale mapping of a joint network (Hornelen Basin, Norway), *Journal of Geophysics Research*, **107** (2002).

Caine, J., Evans, J., and Forster, C.: Fault zone architecture and permeability structure. *Geology*, **24** (1996), 1025–1028.

Cembrano, J., Hervé, F., and Lavenu, A.: The Liquiñe Ofqui fault zone: a long-lived intra-arc fault system in southern Chile. *Tectonophysics*, **259** (1996), 55–66.

Chester, F. M., and Logan, J. M.: Implications for Mechanical-Properties of Brittle Faults from Observations of the Punchbowl Fault Zone, California. *Pure and Applied Geophysics*, **124** (1986), 79–106.

Cox, S. F.: Deformational controls on the dynamics of fluid flow in mesothermal gold systems. *Geological Society, London, Special Publications*, **155** (1999), 123–140

Davy, P., Bour, O., de Dreuzy, J.-R., Darcel, C.: Flow in multiscale fractal fracture networks. *Fractal Analysis for Natural Hazards,* **261** (2006), 31–45.

Faulkner, D. R., Jackson, C. A. L., Lunn, R. J., Schlische, R. W., Shipton, Z. K., Wibberley, C. A. J., and Withjack, M. O.: A review of recent developments concerning the structure, mechanics and fluid flow properties of fault zones. *Journal of Structural Geology*, **32** (2010), 1557–1575.

Faulkner, D. R., Lewis, A. C., and Rutter, E. H.: On the internal structure and mechanics of large strike-slip fault zones: Field observations of the Carboneras fault in southeastern Spain. *Tectonophysics*, **367** (2003), 235–251.

Faulkner, D. R., and Rutter, E. H.: Can the maintenance of overpressured fluids in large strike-slip fault zones explain their apparent weakness, *Geology*, **29** (2001), 503–506.

Gomila, R., Arancibia, G., Mitchell, T. M., Cembrano, J., Faulkner, D.: Paleopermeability structures within Fault-damage zones: A snap-shot from microfracture analyses in a strike-slip system. *Journal of Structural Geology.* **83** (2016), 103-120.

Gudmundsson, A., Berg, S. S., Lyslo, K. B., and Skurtveit, E.: Fracture networks and fluid transport in active fault zones. *Journal of Structural Geology*, **23** (2001), 343–353.

Healy, D., Rizzo, R., Cornwell, D., Farrell, N., Watkins, H., Timms, N., Gomez-Rivas, E., Smith, M.: FracPaQ: A Matlab™ toolbox for the quantification of fractures patterns, *Journal of Structural Geology*, **95** (2017), 1-16.

Heap, M. J., Faulkner, D. R., Meredith, P. G., and Vinciguerra, S.: Elastic moduli evolution and accompanying stress changes with increasing crack damage: Implications for stress changes around fault zones and volcanoes during deformation. *Geophysical Journal International*, **183** (2010), 225–236.

Held, S., Schill, E., Schneider, J., Nitschke, F., Morata, D., Neumann, T., and Kohl, T.: Geochemical characterization of the geothermal system at Villarrica volcano, Southern Chile; Part 1: Impacts of lithology on the geothermal reservoir. *Geothermics*, **74** (2018), 226–239.

Lahsen, A., Muñoz, N., and Parada, M. A.: Geothermal Development in Chile. *Proceedings World Geothermal Congress*, (2010). 25–29.

Lara, L. and Moreno, H.: Geología del área Liquiñe-Neltume. Regiones de Los Lagos y de La Araucanía. servicio Nacional de Geología y Minería. Carta Geológica de Chile, Serie Geología Básica, **83** (2004)., p. 23, 1 mapa 1:100.000

Long, J. C. S and Billaux, D. M.: From field data to fracture network modeling: An example incorporating spatial structure, *Water Resource*, **23(7)** (1987), 1201 – 1216.

Manzocchi, T.: The connectivity of two-dimensional networks of spatially correlated fractures. *Water Resources Research*, **38** (2002).

Melnick, D., Rosenau, M., Folguera, A., and Echtler, H.: Neogene tectonic evolution of the Neuquén Andes western flank. *Evolution of an Andean Margin: A Tectonic and Magmatic View from the Andes to the Neuquén Basin (35°-39°S Lat)*, **2407** (2006), 73–95.

Moeck, I. S.: Catalog of geothermal play types based on geologic controls. *Renewable and Sustainable Energy Reviews*, **37** (2014), 867–882.

Munizaga, F., Herve, F., Drake, R., Pankhurst, R. J., Brook, M., and Snelling, N.: Geochronology of the Lake Region of south-central Chile (39-42 °S): Preliminary results. *Journal of South American Earth Sciences*, **1(3)** (1988), 309–316.

Nyberg, B., Nixon, C. W., and Sanderson, D. J.: NetworkGT: A GIS tool for geometric and topological analysis of two-dimensional fracture networks. *Geosphere*, **14** (2018).

Pankhurst, R. J., Hervé, F., Rojas, L., and Cembrano, J.: Magmatism and tectonics in continental Chiloe, Chile. *Tectonophysics*, **205** (1992), 283–294.

Pankhurst, R. J., Weaver, S. D., Hervé, F., and Larrondo, P.: Mesozoic – Cenozoic evolution of the North Patagonian Batholith in Aysén, southern Chile. *Journal of the Geological Society*, **156** (1999)., 673–694.

Pérez-Flores, P., Cembrano, J., Sánchez-Alfaro, P., Veloso, E., Arancibia, G., and Roquer, T.: Tectonics, magmatism and paleo-fluid distribution in a strike-slip setting: Insights from the northern termination of the Liquiñe–Ofqui fault System, Chile. *Tectonophysics*, **680** (2016), 192-210.

Rohrbaugh, M., Dunne, W., Mauldon, M.: Estimating fracture trace intensity, density and mean length using circular scan lines and windows. *AAPG Bulletin*, **82** (2002), 12, 2089-2104.

Rosenau, M., Melnick, D., and Echtler, H.: Kinematic constraints on intra-arc shear and strain partitioning in the southern Andes between 38°S and 42°S latitude. *Tectonics*, ***25*(4)** (2006).

Sánchez, P., Pérez-Flores, P., Arancibia, G., Cembrano, J., and Reich, M.: Crustal deformation effects on the chemical evolution of geothermal systems: The intra-arc Liquiñe-Ofqui fault system, Southern Andes. *International Geology Review*, ***55*(11)** (2013), 1384–1400.

Sanchez-Alfaro, P., Sielfeld, G., Campen, B. Van, Dobson, P., Fuentes, V., Reed, A., Palma- Behnke, R. and Morata, D.: Geothermal barriers, policies and economics in Chile - Lessons for the Andes. *Renewable and Sustainable Energy Reviews*, **51** (2015), 1390–1401.

Sanderson, D. J., and Nixon, C. W.: The use of topology in fracture network characterization. *Journal of Structural Geology*, **72** (2015), 55–66.

Sibson, R. H.: Structural permeability of fluid-driven fault-fracture meshes. *Journal of Structural Geology*, **18(8)** (1996), 1031–1042.

Stanton-Yonge, A., Griffith, W. A., Cembrano, J., St. Julien, R., and Iturrieta, P. (2016). Tectonic role of margin-parallel and margin-transverse faults during oblique subduction in the Southern Volcanic Zone of the Andes: Insights from Boundary Element Modeling. *Tectonics*, *35*(9), 1990–2013.

Tardani, D., Reich, M., Roulleau, E., Takahata, N., Sano, Y., Perez-Flores, P., Sánchez-Alfaro, P., Cembrano, J., Arancibia, G.: Exploring the structural controls on helium, nitrogen and carbon isotope signatures in hydrothermal fluids along an intra-arc fault system. *Geochimica Et Cosmochimica Acta*, **184** (2016), 193–211.

Watkins, H., Bond, C., Healy, D., Butler, R.: Appraisal of fracture sampling methods and new workflow to characterize heterogeneous fracture network at outcrop. Journal of Structural Geology, **72** (2015), 67-82.